Enhanced antitumor immunity by targeting dendritic cells with tumor cell lysate-loaded chitosan nanoparticles vaccine

Gao-Na Shi[a,1], Chuang-Nian Zhang[a,1], Rong Xu[b], Jin-Feng Niu[c], Hui-Juan Song[a], Xiu-Yuan Zhang[a], Wei-Wei Wang[a], Yan-Ming Wang[c], Chen Li[a,**], Xiao-Qing Wei[d,***], De-Ling Kong[a,e,*]

[a] *Tianjin Key Laboratory of Biomaterial Research, Institute of Biomedical Engineering, Chinese Academy of Medical Science & Peking Union Medical College, Tianjin, 300192, China.*

[b] *Department of Clinical Infection Microbiology and Immunology, Institute of Infection and Global Health, University of Liverpool, L69 7BE, UK.*

[c] *State Key Laboratory of Medical Chemical Biology, College of Pharmacy and Tianjin Key Laboratory of Molecular Drug Research, Nankai University, 300353, China*

[d] *Cardiff Institute of Tissue Engineering & Repair, School of Dentistry, College of Biomedical and Life Sciences, Cardiff University, UK.*

[e] *Key Laboratory of Bioactive Materials, Ministry of Education, Nankai University, Tianjin 300071, China*

[*] **Corresponding authors**

[**] **Corresponding authors**

[***] **Corresponding authors**

E-mail address: li0616826@126.com (C.Li), weiX1@cardiff.ac.uk (X-Q, Wei), kongdeling@nankai.edu.cn (D-L, Kong) .

[1] Gaona Shi and Chuangnian Zhang contributed equally to this work.

Abstract

Whole tumor cell lysates (TCL) have been implemented as tumor antigens for cancer vaccine development, although clinical outcomes of TCL-based antitumor immunotherapy remain unsatisfactory. In order to improve the efficacy of TCL-based vaccines, biomaterials have been employed to enhance antigen delivery and presentation. Here, we have developed chitosan nanoparticles (CTS NPs) with surface mannose (Man) moieties for specific dendritic cells (DCs) targeting (Man-CTS NPs). The Man-CTS NPs were then loaded with TCL generated from B16 melanoma cells (Man-CTS-TCL NPs) for *in vitro* and *in vivo* assessment. Potency of the Man-CTS-TCL NPs as cancer vaccine was also assessed *in vivo* by immunization of mice with Man-CTS-TCL NPs followed by re-challenge with B16 melanoma cell inoculation. We have shown here that Man-CTS-TCL NPs promote bone marrow-derived dendritic cells (BMDCs) maturation and antigen presentation *in vitro*. *In vivo* evaluation further demonstrated that the Man-CTS-TCL NPs were readily taken up by endogenous DCs within the draining lymph node (DLN) following subcutaneous administration accompanied by increase in serum IFN-γ and IL-4 levels. Tumor growth was also significantly delayed in mice primed with Man-CTS-TCL NPs vaccine, attributable at least in part to cytotoxic T lymphocytes response. Moreover, Man-CTS-TCL NPs vaccine also exhibited therapeutic effects in mice with melanoma. Thus, we report here the Man-CTS-TCL NPs as effective anti-tumor vaccine for cancer immunotherapy.

***Keywords*:** Dendritic cell targeting; Immunotherapy; Tumor cell lysates; Nano-vaccine; Chitosan

1. Introduction

Cancer immunotherapy is now considered a promising therapeutic approach against melanoma, leukemia, prostate and breast cancer [1-3]. The main purpose of this strategy is to prime naïve T cells and evoke long-term memory $CD8^+$ T cells that attack tumor cells. Sufficient tumor antigen presentation, often by the antigen presenting cells (APCs) via the major histocompatibility complex (MHC) class I or II pathways, is critical in eliciting effective activation of both $CD8^+$ and $CD4^+$ T lymphocytes and thus determines the therapeutic efficacy of antitumor immunotherapy [4-6].

Dendritic cells (DCs) are professional antigen presenting cells (APCs) and are experts in priming T cells-mediated immunity [7,8]. DCs-based vaccine has been extensively investigated as a feasible approach to enhance antigen-specific immune responses [6]. Most previous studies aimed at developing tumor vaccines that activate cytotoxic T lymphocytes (CTLs) responses and antibody secreting B cells through DCs mediated antigen presentation [9,10]. However, despite promising preliminary data, clinical outcomes of tumor vaccines have been disappointing [11,12]. One major challenge of the current antitumor immunotherapy is inefficient antigen delivery and subsequent induction of T cell mediated immune responses. In addition, the electrofusion process of DCs and tumor cells is time-consuming and laborious [13]. Moreover, external pulsing of DCs with selective peptides only results in limited stimulation of T cells due to the rapid turnover of class I peptides complex on the cell surface [14].

It has been recently shown that the use of whole tumor cell lysates preparation can overcome the above drawbacks and offers a comprehensive source of potential tumor antigens by inducing CTL responses and $CD4^+$ T helper cell activation [15,16]. Several clinical trials have used tumor cell lysates for *in vitro* DC priming [17,18]. However, soluble tumor lysates containing antigens and cytokines are inherently unstable and tend to result in poor DCs uptake, inefficient antigen cross-presentation, and limited induction of CTL response [19]. Recent strategies for developing prophylactic or therapeutic vaccines have mainly focused on improving *in vivo* antigen delivery to specific DCs and prolonging their activation.

Biomaterial encapsulation of antigens has been proposed as a promising strategy to enhance immunogenicity during vaccination [20]. Not only could biomaterial encapsulation protect the antigens from degradation during *in vivo* administration, it also enables controlled release of antigens in a desired manner [21-24]. Moreover, surface of biomaterials could be modified with ligands or antibodies that are specifically recognized by DCs and used for DC targeting [25].

Chitosan is a cationic polysaccharide primarily derived from the exoskeletons of crustaceans and extensively used as vaccine delivery vehicles [21,26,27]. Earlier studies have reported chitosan-based nanoparticles, with particle size ranging from 100 to 500 nm, as feasible vehicles for *in vivo* delivery of proteins or peptides [28]. Moreover, chitosan nanoparticles have been reported to elicit significant adjuvant effect by stimulating innate immune responses [29]. Given the potential pro-inflammatory property of chitosan, we have developed chitosan nanoparticles

with surface-decorated mannose (Man-CTS NPs) for specific DC targeting. Indeed, studies have shown that nanoparticles with surface-decorated mannose are effective delivery vehicles for APCs targeting [30-32]. Since the mannose receptor is expressed by immature dendritic cells, the mannose moiety on the surface of the Man-CTS NPs can be detected by DCs, via which antigen uptake would be enhanced [33,34]. Thus, in the present study, targeted delivery of Man-CTS-TCL NPs was assessed both *in vivo* and *in vitro*. In addition, to evaluate the potential of Man-CTS NPs as cancer vaccine delivery vehicle, we also encapsulated tumor cell lysates generated from B16 melanoma cells (Man-CTS-TCL NPs) and *in vivo* assessment of Man-CTS-TCL NPs on tumor prevention was performed.

2. Material and methods

2.1. Reagent and antibodies

Chitosan (CTS, Mw = 50,000, DD (degree of deacetylation) > 95%) was supplied by Ao'xing Biotechnology Co., Ltd. (Zhejiang, China), and used without further purification. Sodium alginate (ALG, viscosity: 160 mpa·s, 20 ℃, 1% aqueous solution) was supplied by Qingdao Crystal Rock Biology Development Co., Ltd. (Qingdao, China). Tetrabutylammonium (TBA) hydroxide and 4-Aminophenyl α-D-mannopyranoside (MAN) were purchased from Aladdin (Shanghai, China). 2-chloro-1-methylpyridinium iodide (CMPI) was obtained from Alfa Aesar (Tianjin, China). Sodium sulfate, polysorbate 80 (Tween 80) and acetic acid were purchased from Sigma (St. Louis, MO). The MicroBCA™ Protein assay kit was supplied by Thermo Fisher Scientific Inc. (Rockford, IL USA). Phosphate Buffered Saline (PBS)

(1×), RPMI-1640 medium, heat inactivated fetal bovine serum (FBS), trypsin EDTA 0.05%, penicillin/streptomycin (PEST) 10,000 Unit/mL/10,000 μg/mL, sodium pyruvate 100 mM, HEPES 1 M, 2-mercaptoethanol 50 mM, ACK lysing buffer and AlamarBlue® reagent were purchased from Life Technologies (Carlsbad, CA, USA). All the other chemicals were of analytical grade.

Anti-mouse ELISA kits IFN-γ, IL-4, IgG and IL-12p70 were purchased from eBioscience. Recombinant mouse GM-CSF and IL-4 were purchased from Peprotech (Rocky, Hill, USA). Fluorochrome-labeled anti-mouse monoclonal antibodies (CD3e, CD4, CD8a, CD80, CD86, MHCI, MHCII, CD11c, CD40 and CCR7) were purchased from eBioscience (CA, USA).

2.2. Cell lines and animals

Female C57BL/6 (6-8 weeks old) and female Balb/c mice (6-8 weeks old) were purchased from (Academy of Military Medical Sciences, Beijing, China). All animal procedures were reviewed and ethically approved by Center of Tianjin Animal Experiment ethics committee and authority for animal protection (Approval No.: SYXK (Jin) 2011-0008). Mouse B16 melanoma tumor cell line [35] was purchased from the Cell Bank of China Academy of Sciences, and cultured according to the manufacture's guidelines.

2.3. Generation and isolation of tumor cell lysates

Tumor cell lysates (TCL) were generated as previously described [36]. Briefly, B16 melanoma tumor cell pellets were re-suspended in ice cold phosphate-buffered saline (PBS) at a 1×10^7/ml cell density and subjected to five freeze-thaw cycles of rapid

freezing in liquid nitrogen (for 5 min) and thawing at 37 □ (for 5 min). The lysates were then centrifuged at 2,000 g for 10 min to remove cellular debris. Protein concentrations were measured by BCA assay and the concentrated protein solution was diluted to appropriate concentration for *in vivo* and *in vitro* experiments.

2.4. Preparation of mannose-modified alginate (Man-ALG)

Tetrabutylammonium-alginate (ALG-TBA) was synthesized as previous report [37]. 500 μg (1.190 mmol) ALG-TBA was dissolved in 50 mL of anhydrous dimethylformamide (DMF). 152.1 mg CMPI (0.595 mmol) was added to activate the ALG-TBA in nitrogen at 0 □. After 1 h, 4-Aminophenyl α-D-mannopyranoside (0.357 mmol) was added at room temperature and leave to react for 24 h. The reaction mixture was precipitated in absolute ethanol, repeatedly dissolved and precipitated for three times. The Man-ALG solution was transferred to a dialysis bag (MW=3500 Da) to dialyze in distilled water for 2 days. The final product of Man-ALG was obtained after freeze-drying. The chemical structure of Man-ALG was confirmed by ^{1}H NMR spectroscopy (Varian Mercury 400, USA) and IR spectroscopy (Spectrum Instruments Co., Ltd. Brook Germany). The substitution degree (SD) of Man was defined as the ratio of reacted sugar unit to the total sugar unit of ALG.

2.5. Preparation and characterization of mannose-decorated chitosan nanoparticle encapsulation of tumor cell lysates (Man-CTS-TCL NPs)

Chitosan and tumor cell lysates (TCL) were dissolved in 1% acetic acid and ultrapure water, respectively. One mg/mL of chitosan solution and 1 mg/mL of TCL were obtained. The TCL solution was added drop-by-drop into chitosan solution and

mixed at 1:1 (w/w). The mixture was then agitated at 300 rpm for 30 min to obtain chitosan/tumor cell lysates complex, which were collected by centrifugation and dissolved in PBS for experimental use. The Man-ALG solution (1 mg/ml) was added drop-by-drop into CTS-TCL NPs suspension to obtain mannose decorated CTS-TCL NPs (Man-CTS-TCL NPs) through electrostatic interaction. Man-CTS-TCL NPs were collected by centrifugation and suspended in PBS (pH 7.4) for further use. The same protocol was followed for CTS-TCL NPs preparation except alginate (1 mg/ml) was added instead of Man-ALG. The method for CTS NPs and Man-CTS NPs is the same with Man-CTS-TCL NPs although TCL was not added for CTS NPs and Man-CTS NPs.

Morphology of the nanoparticles was determined by transmission electron microscopy (TEM, Philips-FEI TecnaiT10, USA). The average particle size, size distributions, and surface charges of nanoparticles were measured respectively by a 90plus particle sizer and Zeta potential analyzer (Nano-ZS 90, Malvern Instrument, UK).

2.6. Assessment of antigens release from Man-CTS-TCL NPs

The amount of TCL released from Man-CTS-TCL NPs was measured under acidic (pH 5.0) and neutral (pH 7.4) condition. Four mg of Man-CTS-TCL NPs were suspended in 4 mL of PBS and incubated at 37 □ with continuous agitation in an orbital shaker. The suspension was centrifuged at 12000 rpm for 10 min at designated time points. Three mL of supernatants were collected and stored at -80 □ for assaying later. Then 3 mL of fresh PBS was added to the original tube for further incubation.

Supernatant samples were tested for total protein using BCA protein assay according to the manufacturer's instruction. Absorbance at 562 nm was measured using a microplate reader (Varioskan LUX multimode reader, Thermo Scientific, USA); proteins concentration was calculated according to standard curve. Cumulative release was studied for 72 h. The amount of proteins released at different time points was also calculated respectively.

2.7. Generation and stimulation of bone marrow derived dendritic cells (BMDCs) *in vitro*

BMDCs were isolated from hind limb bones of mice using published protocol [38,39]. Briefly, both distal bone ends were excised and the marrow cells were flushed using RPMI 1640 (Gibco, Grand Island, NY). The red blood cells were lysed and the remaining cells were centrifuged at 1500 rpm for 10 min. 2×10^6/mL cells were aliquoted in RPMI 1640 supplemented with 10% FBS, 2 mmol/L L-glutamine, 1 mmol/L sodium pyruvate, 100 U/mL penicillin, 100 μg/mL streptomycin, 20 ng/mL of GM-CSF (PeproTech) and 10 ng/mL of IL-4 (PeproTech) at 37 □. Cells were cultured in six-well plates in complete medium with cytokines at 4×10^6 cells/2 mL/well. At day 5 of culturing, TCL, Man-CTS NPs or Man-CTS-TCL NPs were added to make final concentration of 10 μg/ml, and cultured for 2 more days. On day 7, most of the non-adherent cells have acquired typical dendritic morphology, and these cells were used as the source of DCs in subsequent experiment. At this time point supernatant from different cultures were collected and stored at -80 □ for cytokines determination.

For flow cytometry, cells cultured for 7 days were rinsed three times with PBS and

briefly trypsinized to form a single cell suspension. Cells were stained for 30 min on ice with following fluorescence-labeled antibodies (1 μg/2×10^6 cells): Anti-mouse MHCI (H-2Kb)-FITC (clone: AF6-88.5.5.3), Anti-mouse MHCII (clone: AF6-120.1), Anti-mouse CD11c PE-Cy7 (clone: N418), Anti-mouse CD86 APC (clone: GL1), Anti-mouse CD80 FITC (clone: 16-10A1), Anti-mouse CD40 PE (clone: 1C10), Anti-mouse CCR7 PE (clone: 4B12). Cells were then washed twice with cold PBS and analyzed on a four color BD Accuri C6. Data analysis was performed using BD Accuri C6 software (BD biosciences, San Jose, CA).

2.8. Flow cytometry analysis of antigens uptake by BMDCs and the intracellular localization of antigen in BMDCs

The methods for FITC-labeled TCL (TCL-FITC), TCL-FITC loaded CTS nanoparticles (CTS-TCL-FITC NPs) and TCL-FITC loaded Man-CTS nanoparticles (Man-CTS-TCL-FITC NPs) preparation are detailed in supporting information.

Immature BMDCs were cultured with TCL-FITC, CTS-TCL-FITC NPs or Man-CTS-TCL-FITC NPs at 37 □ for 2, 4, 6, 12, 24 and 48 h. The surface binding of TCL-FITC by BMDCs was determined by measuring mean fluorescence intensity (MFI) using flow cytometry.

BMDCs (1×10^6 cells/mL) were cultured with TCL-FITC, CTS-TCL-FITC NPs or Man-CTS-TCL-FITC NPs at 37 □ for 4 h. At the end of the experiment, the cells were labeled with 50 nM Lyso Traker Red DND-99 (Invitrogen, CA, USA) for 60 min to visualize late endosomes and lysosomes. The nuclei were stained with DAPI (Sigma, MO, USA) for 5 min and fluorescent images were recorded by a confocal

laser scanning microscopy (TCS SP5II, Leica, Ernst-Leitz-Strasse, Germany).

2.9. *In vivo* trafficking analysis of Man-CTS-TCL NPs

Near-Infrared Cyanine 7 dyes were used to label TCL. The methods of Cy7 labeled TCL (TCL-Cy7), TCL-Cy7 loaded CTS nanoparticles (CTS-TCL-Cy7 NPs) and TCL-Cy7 loaded Man-CTS nanoparticles (Man-CTS-TCL-Cy7 NPs) preparation are included in supporting information.

Balb/c mice were injected subcutaneously with TCL-Cy7 (50 μg), CTS-TCL-Cy7 NPs containing 50 μg TCL-Cy7 or Man-CTS-TCL-Cy7 NPs containing 50 μg TCL-Cy7 dispersed in 100 μl PBS. Vaccine kinetics was then studied at several time points after administration by a small animal *in vivo* imaging system (Maestro, CRI USA). Mice were anesthetized by inhalation of isoflurane and fluorescence spectral cubes were acquired using near infrared (illumination light from 700 nm to 900 nm in 10 nm steps at 2 s exposure for each step Exp.700 nm to 760 nm, Emission 800 nm long pass) preset filter combinations. Unmixed images in which background signals were subtracted and quantified by using Maestro software. Kinetics was measured by quantifying the fluorescent intensity in pre-set regions of interest (ROI) at the injection site and the draining inguinal lymph node. The fluorescence signal in the injection site at each time point was presented as the percentage of the maximum recorded value, to show percent decrease in time [40].

2.10. *In vivo* immunization, cytokines secretion, and T lymphocytes proliferation assay

C57BL/6 mice were immunized 3 times with PBS (control), TCL, CTS NPs,

Man-CTS NPs, CTS-TCL NPs and Man-CTS-TCL NPs group by subcutaneous (*s.c.*) injection at days -14, -13 and -7. The dose of TCL in each group was 100 μg/mouse. Blood was collected 7 days after last immunization for cytokines and antibody analysis, cytokines of IFN-γ, IL-4, IL-12p70 and TCL antigens specific IgG antibody in serum was determined by ELISA (eBioscience). For analysis of tumor specific IgG antibody, using 10 μg/mL total tumor cell lysates coating the plate to test tumor antigens specific IgG antibody.

For *in vitro* T lymphocytes proliferation assay, splenic T cells were isolated from C57BL/6 mice of all treatment groups 7 days after last immunization and labeled with 5 μmol/L 5, 6-carboxyfluorescein acetate N-succinimidyl ester (CFSE, Sigma-Aldrich) according to the manufacturer's instructions. The CFSE-labeled T cells (4×10^6 cells/mL) were then incubated with 10 μg/mL soluble TCL antigens for re-stimulation of antigen-specific memory T cells responses and maintained in culture for 5 days. T cells were then collected and T lymphocyte proliferation was assessed by flow cytometry. Percentages of $CD4^+$ $CFSE^{low}$ and $CD8^+$ $CFSE^{low}$ T cells were analyzed.

2.11. Immunization and tumor challenge

Female C57BL/6 6-8 weeks old mice were randomized into one of the following treatment groups (n=6): (1) Control group, (2) TCL group, (3) CTS NPs group, (4) Man-CTS NPs group, (5) CTS-TCL NPs group and (6) Man-CTS-TCL NPs group. Mice received 3 subcutaneous injections of 100 μL (concentration was 1 mg/mL) of vaccine at days -14, -13 and -7 in the left flank followed by inoculation with 1×10^5 B16 cells suspended in 50 μL PBS in the right side. The day of inoculation was

counted as day 0 followed by the closely monitored at every other day for pain/distress, tumor volume and body weight. Tumor growth was evaluated by measuring two perpendicular tumor dimensions using a caliper. Tumor volumes (V, mm^3) were calculated using the following formula: $V=1/2(W^2 \times L)$, where W (width) is the perpendicular dimension to the length, L (length) is the longest dimension. Mice were sacrificed at day 21. Tumors were removed and weighted. Spleen and lymph nodes were excised and made into single cells suspension for flow cytometer analysis of T cells subpopulations.

2.12. CTL assays

Single cell suspensions of splenocytes were prepared from mice 21 days after B 16 melanoma cell inoculation. Cells were seeded onto 6-well plates (~1×10^7 cells/well) and co-cultured with B16 cells (~1×10^6 cells/well) for 72 hours. The appropriate numbers of effector (E) cells were incubated with 6000 fresh target (T) B16 cells with E:T ratios varied at 10:1 to 50:1 in each well of U-bottomed 96 well plates. The mixture were then incubated for 4 h at 37 ℃ in 95% O_2/5% CO_2 and the lactate dehydrogenase levels in cell culture supernatants were tested by CTL assay kit following the manufacture's (Promega) instruction [41, 42].

2.13. In vivo assessment of antitumor effect of the M-CTS-TCL NPs

Female C57BL/6 6-8 weeks old mice were s.c. injected in the right flanks with 1×10^5 B16 cells suspended in 50 μL PBS. On day 7, mice were randomly assigned into six groups (n=6 in each group). On day 7, 14, and 21 post tumor inoculation, mice were s.c. immunized with PBS (Group 1), TCL (Group 2), CTS NPs (Group 3),

Man-CTS NPs (Group 4), CTS-TCL NPs (Group 5) and Man-CTS-TCL NPs (Group 6). The day on which B16 melanoma cell inoculation was performed as day 0. Mice were closely monitored every other day for pain/distress, tumor volume and body weight. Tumor growth was evaluated by measuring two perpendicular tumor dimensions using a caliper. Tumor volumes (V, mm3) were calculated using the following formula: V=1/2(W2×L), where W (width) is the perpendicular dimension to the length, L (length) is the longest dimension. Mice were sacrificed at day 22. Sera were collected for IFN-γ and IL-4 ELISA analysis. Tumors were removed and weighted and spleens were excised for flow cytometer analysis of T cells subpopulations.

2.14. Statistical analysis

Data are presented as mean ± standard deviations. The differences between the control group and experimental groups were assessed using a student's t-test, and the differences between groups were determined by one-way ANOVA and Tukey's posttest (GraphPad Software, La Jolla, CA, USA).

3. Results and Discussion

3.1. Preparation and Characterization of Man-CTS-TCL NPs

Due to its anionic property, CTS NPs was synthesized for TCL encapsulation, forming a CTS-TCL complex, which was further coated with mannose-modified alginate (Man-ALG). The synthesis route of Man-ALG is shown in (Fig.1A) and the structure of Man-ALG was confirmed by FT-IR (Fig.1B). As clearly shown in Fig. 1B, the peaks observed at 1616 cm^{-1} and 1418 cm^{-1} are characteristic carboxylate of the

absorption bands of ALG. After mannose modification, the peaks at 1670 cm^{-1} (amide band I) and 1510 cm^{-1} (amide band II) could be observed, indicating formation of amide bonds. Fig.1C shows the ^{1}H NMR spectra of ALG and Man-ALG. Small peaks shown at 7.0-7.5 ppm are representative of typical protons of the 4-Aminophenyl α-D-mannopyranoside moiety, demonstrating successful conjugation of Man to ALG. The substitution degree of Man in Man-ALG was 8.4%, i.e. an average of 8.4 Man moieties per 100 sugars units of ALG.

Physical characteristics of nanoparticles, including the average particle size, size distributions, and surface charges of nanoparticles were summarized in Supporting Information (Table S1). The average diameter of Man-CTS-TCL NPs was 120 nm and spherical in shape with an overall charge of -12 mV (Fig.1D&E). The protein releasing kinetics was determined in vitro and shown in Fig.1F, elevated and more sustained protein release could be detected when the surrounding pH values was 5.0, suggesting a better releasing property of the Man-CTS-TCL NPs in the acidic environment of the endo/lysosomes.

3.2. Man-CTS-TCL NPs promoted antigen uptake in BMDCs

The efficacy of Man-CTS-TCL NPs on antigen uptake was initially examined in BMDCs. TCL-FITC, CTS-TCL-FITC NPs and Man-CTS-TCL-FITC NPs were incubated with BMDCs for 2, 4, 6, 12, 24 or 48 h. Antigen uptake partly through surface binding was quantified by MFI of FITC as measured flow cytometry. Cellular localization of TCL-FITC was examined by confocal fluorescent microscopy. As shown in Fig. 2B&C, a 3-fold increase of FITC-TCL uptake was observed in BMDC

co-cultured with Man-CTS-TCL-FITC NPs as compared controls (MFI: 82.0339± 9.0000 [$\times 10^4$]). As expected, the fluorescence signal of FITC which corresponds to DC antigen uptake decreased over time in all groups. These results suggest that compared to TCL and CTS-TCL NPs, Man-CTS-TCL NPs can significantly increase antigens uptake of BMDCs, partly via enhanced surface binding. In addition, for clarification fluorescence spectra of TCL-FITC, CTS-TCL-FITC NPs and Man-CTS-TCL-FITC NPs are presented in supporting information (Fig. S1).

3.3. Man-CTS-TCL NPs induce BMDC maturation

To further investigate the effect of Man-CTS-TCL NPs on DCs *in vitro*, immature BMDCs were harvest on day 5 after isolation and exposed to Man-CTS-TCL NPs for 48 h. Fig.3A&B shows the microscopic views of mature DCs in microscope. DC maturation was characterized by surface marker expression using flow cytometry, and we found that exposure to Man-CTS-TCL NPs significantly enhanced expression levels of CD80, CD86 and CD40, surface markers that indicates DC maturation (Fig.3C&D). Moreover, the expression levels of MHC I, MHC II, and CCR7 were also upregulated in DCs treated with Man-CTS-TCL NPs (Fig.3E&F), all of which are demonstrative of a facilitative role of Man-CTS-TCL NPs on DC maturation.

3.4. *In vivo* imaging of Cyanine 7 labeled Man-CTS-TCL NPs

In order to investigate the effect of Man-CTS-TCL NPs on endogenous DC activities, TCL-Cy7, CTS-TCL-Cy7 NPs and Man-CTS-TCL-Cy7 NPs were administrated by subcutaneous (*s.c*) injection at the tail base site and the presence of TCL-Cy7, CTS-TCL-Cy7 NPs and Man-CTS-TCL-Cy7 NPs were then visualized at

the injection site and in the adjacent draining lymph node (DLN), where immune responses are initiated [43]. We selected tail base as injection site which is able to distinguish from the lymph nodes and it drains specifically to the inguinal lymph node (ILN) [44]. Fig.4A shows representative images of fluorescence signals corresponding to TCL-Cy7, CTS-TCL-Cy7 NPs and Man-CTS-TCL-Cy7 NPs at the injection site and the ILN (Fig.4A red arrows) at designated time points. The fluorescence signals were quantified and the average fluorescence were plotted against time and presented in Fig.4B. Improved migratory ability of Man-CTS-TCL-Cy7 NPs to the ILN was evident as compared to TCL-Cy7 and CTS-TCL-Cy7. Furthermore, accumulation of free TCL was observable in the liver of TCL-only group whilst for CTS-TCL NPs group; the fluorescence signal was detected not just within the ILN, but also in adjacent tissues. No signal of Cy 7 could be recorded in the ILN at 24 h following injection in both TCL and CTS-TCL NPs group, in contrast to the Man-CTS-TCL NPs group, where robust and sustained Cy 7 signal was detectable at 24 h following injection. One explanation for the migratory advantage of Man-CTS-TCL-Cy7 NPs is that both active and passive pathways are involved during antigen migration from the tail back to the right inguinal DLN [28]. This is consistent with previous study reporting that nanoparticles with comparatively smaller size facilitate DC uptake by passive cellular endocytosis [45]. Since the average size of Man-CTS-TCL NPs is approximately 100 nm, it is possible that the nanoparticles are taken up by resident DCs passively in addition to active uptake as a result of the mannose interaction.

3.5. Effect of Man-CTS-TCL NPs on endogenous DCs maturation and antigen

presentation at the draining lymph node

To assess the efficacy of Man-CTS-TCL NPs as potential cancer vaccine, mice were administrated with Man-CTS-TCL NPs, CTS-TCL NPs, Man-CTS NPs, CTS NPs or TCL only by *s.c.* injection at days -14, -13 and -7. Non-treated mice were also included in parallel as controls. On day 0 and day 7, the draining lymph nodes and spleen of each mouse were obtained. As shown in Fig.5A, the ILNs from CTS-TCL NPs group and Man-CTS-TCL NPs group were moderately bigger in size compared to other groups. DC maturation is associated with a wide range of cellular changes, such as increased expression of costimulatory molecules, surface MHC class II molecules, and chemokine receptor (e.g. CCR7), which allow them to migrate to the LNs [4]. To assess the impact of nanoparticle-delivered TCL antigen on DC maturation, expression levels of CD11c, CD80, CD86, MHCII and CCR7 on APCs within the ILNs were analyzed. It is clear from Fig.5B, expressions of $CD11c^+CD86^+$, $CD11c^+CD80^+$, $CD11c^+MHCII^+$, $CD11c^+MHCI^+$ and $CD11c^+CCR7^+$ were upregulated in the Man-CTS-TCL NPs group, significantly elevated as compared to other groups, indicating more robust impact of the Man-CTS-TCL NPs on stimulating resident DC maturation within the LNs. Furthermore, results of antigen recall T-cell proliferation also showed that proliferation of both $CD8^+$ and $CD4^+$ T cells were elevated from the Man-CTS-TCL NPs exposed group when compared to others. Proliferation of $CD8^+$ T cells were significantly increased compared with CTS NPs and Man-CTS NPs, but not the TCL only group. Whilst $CD4^+$ T cell proliferation was significantly enhanced from the Man-CTS-TCL NPS when compared with TCL group,

CTS NPs and Man-CTS NPs (Fig.5C&D). Similarly, upregulation of IFN-γ and IL-4 was also detected in the sera of mice (Fig.5E&F), confirming T cell activation.

3.6. Man-CTS-TCL NPs as a nano-vaccine exhibited TCL-induced antitumor immune responses

To examine the antitumor efficacy of Man-CTS-TCL NPs, we immunized C57BL/6 mice with Man-CTS-TCL NPs and re-challenged the mice by inoculation of 1×10^5 B16 tumor cells. The detailed immunization protocol is included in Supplementary Fig.S4A. There was no significant difference in mice body weight among those six groups (Fig.6A). As shown in Fig.6B, administration of Man-CTS-TCL NPs could significantly delay tumor growth compared with untreated control group, CTS NPs group, Man-CTS NPs group and mice immunized with TCL, shown by considerably smaller tumor size by Day 21. What's more, compared with control group, TCL group, CTS NPs group, Man-CTS NPs group, and CTS-TCL NPs group, the average tumor weight in Man-CTS-TCL NPs group was significantly decreased (Fig.6C).

It has been well established that $CD8^+$ T cells are important effector cells in vaccine induced anti-tumor responses [46]. In line with that, we found that mice immunized with Man-CTS-TCL NPs showed significantly more $CD8^+$ T cells in the LN and spleen than other groups (Fig.6E&F). No difference could be detected regarding $CD4^+$ T cells following immunization among all treatment groups (Data not shown). Meanwhile, the absolute number of $CD3^+$ T cells in spleen was calculated and no significant difference could be deduced between Man-CTS-TCL NPs group and others (Supplementary Fig.S4B). Significant elevation of the absolute number of

$CD3^+CD8^+$ T cells in spleen was seen in the Man-CTS-TCL NPs group when compared with others (Supplementary Fig.S4C), all of which emphasize the importance of $CD8^+$ T cells in Man-CTS-TCL NPs-induced antitumor activity.

3.7. Man-CTS-TCL NPs potently enhanced cytotoxic T lymphocytes (CTL) responses against tumor

To test the efficacy of T cells in mediating tumor-specific CTL responses, cytotoxic T lymphocyte (CTL) assay was performed. First, we co-cultured the effector cells (splenocytes isolated from immunized mice) and the target cells B16 melanoma cells. Lysis of target cells was then tested at the Effector:Target (E:T) cell ratio of 10:1, 20:1 and 50:1. Importantly, the effector T cells isolated from mice immunized with Man-CTS-TCL NPs lysed ~35% target melanoma cells, while the lysed target melanoma cells in control group was only ~12% (Fig.6D). This showed that mice immunized with Man-CTS-TCL NPs were more efficient in inducing CTL response against the B16 melanoma target cells.

3.8. Man-CTS-TCL NPs achieved therapeutic effects in melanoma tumor model

To investigate the therapeutic effect of Man-CTS-TCL NPs, C57BL/6 mice were inoculated *s.c.* with 1×10^5 B16 melanoma cells 7 days before vaccination with Man-CTS-TCL NPs. Detailed protocol is shown in Supplementary Fig.S5A. There was no significant difference in mice body weight among all groups (Fig.7A). As shown in Fig.7B, vaccination with Man-CTS-TCL NPs significantly inhibited B16 tumor growth, compared with PBS-administrated controls. Consistently, tumor weight in Man-CTS-TCL NPs group was significantly decreased at day 22 compared to

control group, although no differences could be observed between other groups and control (Fig 7C). Expression of mouse serum IFN-γ was consistent with the anti-tumor results (Fig.7E). Compared with other groups, mice in Man-CTS-TCL NPs group showed more $CD8^+$ T cells in spleen (Fig.7F), with no difference detectable regarding the absolute number of $CD3^+$ T cells in spleen (Supplementary Fig.S5B). Significant increase of the absolute number of $CD3^+CD8^+$ T cells in spleen was observed in Man-CTS-TCL NPs when compared to others (Supplementary Fig. S5C). These results suggest that Man-CTS-TCL NPs exhibit therapeutic efficacy in mice with melanoma, and it may provide a translational option as immunotherapy.

4. Conclusion

In summary, we demonstrate here chitosan-based nanoparticles with surface -decorated mannose, Man-CTS NPs as potential vehicle for cancer vaccine delivery. Furthermore, by encapsulating TCL generated from B16 melanoma cells, we further showed the Man-CTS-TCL NPs as potent cancer vaccine for tumor prevention. The robust antitumor effect of Man-CTS-TCL NPs could be partly attributed to effective stimulation of cellular and humoral antitumor immunities by the nanoparticles. In addition, we also demonstrate the possibility of using mannose as effective DC targeting ligand by conjugation of mannose with biomaterials to facilitate DC maturation, antigen uptake and presentation. Thus, we report here chitosan-based nanoparticles with surface-decorated mannose as antigen delivery vehicle that improves the efficacy of antitumor immune responses than CTS-TCL NPs and TCL alone. The Man-CTS-TCL NPs could therefore be considered a feasible therapeutic

approach as development of cancer vaccine.

Acknowledgements

This work was supported by the National Natural Science Foundation of China (81301309 and 51373199), Peking Union Medical College Innovation Research Team Fund, Global Innovation Initiative Consortium Fund, and National Fund for Young Investigator (31400833), and Peking Union Medical College Innovation Fund.

References

[1] S.B. Coffelt, K.E. de Visser, Immune-mediated mechanisms influencing the efficacy of anticancer therapies, Trends Immunol. 36 (2015) 198-216.

[2] A.S. Cheung, D.J. Mooney, Engineered materials for cancer immunotherapy, Nano today 10 (2015) 511-531.

[3] A.Milani, D. Sangiolo, F. Montemurro, M. Aglietta, G. Valabrega, Active immunotherapy in HER2 overexpressing breast cancer: current status and future perspectives, Ann. Oncol. 24 (2013) mdt133.

[4] K. Palucka, J. Banchereau, Dendritic-cell-based therapeutic cancer vaccines, Immunity 39 (2013) 38-48.

[5] I. Melero, G. Gaudernack, W. Gerritsen, C. Huber, G. Parmiani, S. Scholl, et al., Therapeutic vaccines for cancer: an overview of clinical trials, Nat. Rev. Clin. Oncol. 11 (2014) 509-524.

[6] J. Banchereau, A.K. Palucka, Dendritic cells as therapeutic vaccines against cancer, Nat. Rev. Immunol. 5 (2005) 296-306.

[7] S.T. Reddy, M.A. Swartz, J.A. Hubbell, Targeting dendritic cells with biomaterials: developing the next generation of vaccines, Trends Immunol. 27 (2006) 573-579.

[8] J. Banchereau, R.M. Steinman, Dendritic cells and the control of immunity, Nature 392 (1998) 245-252.

[9] F.O. Nestle, J. Banchereau, D. Hart, Dendritic cells: on the move from bench to bedside, Nat. Med. 7 (2001) 761-765.

[10] E. Segura, J.A. Villadangos, Antigen presentation by dendritic cells in vivo, Curr. Opin.

Immunol. 21 (2009) 105-110.

[11] V.K. Sondak, J.A. Sosman, Results of clinical trials with an allogeneic melanoma tumor cell lysate vaccine: Melacine®, Semin. Cancer Biol. 13 (2003) 409-415.

[12] P. Livingston, The unfulfilled promise of melanoma vaccines, Clin. Cancer Res. 7 (2001) 1837-1838.

[13] Y. Zhang, B. Ma, Y. Zhou, M. Zhang, X. Qiu, Y. Sui, et al., Dendritic cells fused with allogeneic breast cancer cell line induce tumor antigen-specific CTL responses against autologous breast cancer cells, Breast Cancer Res. Treat. 105 (2007) 277-286.

[14] E. Jäger, M. Ringhoffer, J. Karbach, M. Arand, F. Oesch, A. Knuth, Inverse relationship of melanocyte differentiation antigen expression in melanoma tissues and CD8+ cytotoxic-T-cell responses: evidence for immunoselection of antigen−loss variants in vivo, Int. J. Cancer 66 (1996) 470-476.

[15] H. Zhang, K. Tang, Y. Zhang, R. Ma, J. Ma, Y. Li, et al., Cell-free tumor microparticle vaccines stimulate dendritic cells via cGAS/STING signaling, Cancer Immunol. Res. 3 (2014) 196-205.

[16] C.L.-L. Chiang, F. Benencia, G. Coukos, Whole tumor antigen vaccines, Semin Immunol. 22 (2010) 132-143.

[17] P.G. Coulie, B.J. Van den Eynde, P. van der Bruggen, T. Boon, Tumour antigens recognized by T lymphocytes: at the core of cancer immunotherapy, Nat. Rev. Cancer 14 (2014) 135-146.

[18] L.E. Kandalaft, J. Powell, Daniel J, C.L. Chiang, J. Tanyi, S. Kim, et al., Autologous lysate-pulsed dendritic cell vaccination followed by adoptive transfer of vaccine-primed ex vivo co-stimulated T cells in recurrent ovarian cancer, Oncoimmunology 2 (2013) e22664.

[19] C. Solbrig, J. Saucier-Sawyer, V. Cody, W. Saltzman, D. Hanlon, Polymer nanoparticles for immunotherapy from encapsulated tumor-associated antigens and whole tumor cells, Mol. Pharmaceut. 4 (2007) 47-57.

[20] M.F. Bachmann, G.T. Jennings, Vaccine delivery: a matter of size, geometry, kinetics and molecular patterns, Nat. Rev. Immunol. 10 (2010) 787-796.

[21] M. Garcia-Fuentes, M.J. Alonso, Chitosan-based drug nanocarriers: Where do we stand?, J. Control. Release 161 (2012) 496-504.

[22] X. Xia, J. Mai, R. Xu, J.E.T. Perez, M.L. Guevara, Q. Shen, et al., Porous silicon microparticle potentiates anti-tumor immunity by enhancing cross-presentation and inducing type I interferon response, Cell Rep.11 (2015) 957-966.

[23] Y. Qian, H. Jin, S. Qiao, Y. Dai, C. Huang, L. Lu, et al., Targeting dendritic cells in lymph node with an antigen peptide-based nanovaccine for cancer immunotherapy, Biomaterials 98 (2016) 171-183.

[24] S. Maharjan, B. Singh, T. Jiang, S.Y. Yoon, H.S. Li, G. Kim, et al., Systemic administration of RANKL overcomes the bottleneck of oral vaccine delivery through microfold cells in ileum, Biomaterials 84 (2016) 286-300.

[25] Y.J. Kwon, E. James, N. Shastri, J.M.J. Fréchet, In vivo targeting of dendritic cells for activation of cellular immunity using vaccine carriers based on pH-responsive microparticles, Proc. Natl. Acad. Sci. USA 102 (2005) 18264-18268.

[26] J.J. Moon, H. Suh, A.V. Li, C.F. Ockenhouse, A. Yadava, D.J. Irvine, Enhancing humoral responses to a malaria antigen with nanoparticle vaccines that expand Tfh cells and promote germinal center induction, Proc. Natl. Acad. Sci. USA 109 (2012) 1080-1085.

[27] T. Kambayashi, T.M. Laufer, A typical MHC class II-expressing antigen-presenting cells: can anything replace a dendritic cell?, Nat. Rev. Immunol. 14 (2014) 719-730.

[28] S.T. Reddy, A.J. van der Vlies, E. Simeoni, V. Angeli, G.J. Randolph, C.P. O'Neil, et al., Exploiting lymphatic transport and complement activation in nanoparticle vaccines, Nat. Biotechnol. 25 (2007) 1159-1164.

[29] E.C. Carroll, L. Jin, A. Mori, N. Muñoz-Wolf, E. Oleszycka, Hannah B.T. Moran, et al., The Vaccine Adjuvant Chitosan Promotes Cellular Immunity via DNA Sensor cGAS-STING-Dependent Induction of Type I Interferons, Immunity 44 (2016) 597-608.

[30] J.-S. Thomann, B. Heurtault, S. Weidner, M. Brayé, J. Beyrath, S. Fournel, et al., Antitumor activity of liposomal ErbB2/HER2 epitope peptide-based vaccine constructs incorporating TLR agonists and mannose receptor targeting, Biomaterials 32 (2011) 4574-4583.

[31] R.A. Rosalia, L.J. Cruz, S. van Duikeren, A.T. Tromp, A.L. Silva, W. Jiskoot, et al., CD40-targeted dendritic cell delivery of PLGA-nanoparticle vaccines induce potent anti-tumor responses, Biomaterials 40 (2015) 88-97.

[32] C.L. van Broekhoven, C.R. Parish, C. Demangel, W.J. Britton, J.G. Altin, Targeting dendritic

cells with antigen-containing liposomes: a highly effective procedure for induction of antitumor immunity and for tumor immunotherapy, Cancer Res. 64 (2004) 4357-65.

[33] A.J. Engering, M. Cella, D. Fluitsma, M. Brockhaus, E. Hoefsmit, A. Lanzavecchia, et al., The mannose receptor functions as a high capacity and broad specificity antigen receptor in human dendritic cells, Eur. J. Immunol. 27 (1997) 2417-2425.

[34] F. Sallusto, M. Cella, C. Danieli, A. Lanzavecchia, Dendritic cells use macropinocytosis and the mannose receptor to concentrate macromolecules in the major histocompatibility complex class II compartment: downregulation by cytokines and bacterial products, J. Exp. Med.182 (1995) 389-400.

[35] C.M. Celluzzi, J.I. Mayordomo, W.J. Storkus, M.T. Lotze, L. Falo, Peptide-pulsed dendritic cells induce antigen-specific CTL-mediated protective tumor immunity, J. Exp. Med. 183 (1996) 283-287.

[36] L. Alaniz, M.M. Rizzo, G. Mazzolini, Pulsing dendritic cells with whole tumor cell lysates, Methods Mol. Biol. 1139 (2014) 27-31.

[37] H. Guo, Q. Lai, W. Wang, Y. Wu, C. Zhang, Y. Liu, et al. Functional alginate nanoparticles for efficient intracellular release of doxorubicin and hepatoma carcinoma cell targeting therapy. Int. J. Pharm. 451(2013) 1-11.

[38] M.B. Lutz, N. Kukutsch, A.L. Ogilvie, S. Rößner, F. Koch, N. Romani, et al., An advanced culture method for generating large quantities of highly pure dendritic cells from mouse bone marrow, J. Immunol. Methods 223 (1999) 77-92.

[39] K. Inaba, M. Inaba, N. Romani, H. Aya, M. Deguchi, S. Ikehara, et al., Generation of large numbers of dendritic cells from mouse bone marrow cultures supplemented with granulocyte/macrophage colony-stimulating factor, J. Exp. Med. 176 (1992) 1693-1702.

[40] N. Kosaka, M. Mitsunaga, S. Bhattacharyya, S.C. Miller, P.L. Choyke, H. Kobayashi, Self-illuminating in vivo lymphatic imaging using a bioluminescence resonance energy transfer quantum dot nano-particle, Contrast Media Mol. I. 6 (2011) 55-59.

[41] Q. Rao, B. Zuo, Z. Lu, X. Gao, A. You, C. Wu, et al., Tumor-derived exosomes elicit tumor suppression in murine hepatocellular carcinoma models and humans in vitro, Hepatology 15 (2016) 1-17.

[42] A. Garu, G. Moku, S.K. Gulla, A. Chaudhuri, Genetic Immunization With In Vivo Dendritic

Cell-targeting Liposomal DNA Vaccine Carrier Induces Long-lasting Antitumor Immune Response, Mol. Ther. 24 (2016) 385-397.

[43] M. Sixt, N. Kanazawa, M. Selg, T. Samson, G. Roos, D.P. Reinhardt, et al., The Conduit System Transports Soluble Antigens from the Afferent Lymph to Resident Dendritic Cells in the T Cell Area of the Lymph Node, Immunity 22 (2005) 19-29.

[44] S. Rahimian, J.W. Kleinovink, M.F. Fransen, L. Mezzanotte, H. Gold, P. Wisse, et al., Near-infrared labeled, ovalbumin loaded polymeric nanoparticles based on a hydrophilic polyester as model vaccine: In vivo tracking and evaluation of antigen-specific CD8+ T cell immune response, Biomaterials 37 (2015) 469-477.

[45] V. Manolova, A. Flace, M. Bauer, K. Schwarz, P. Saudan, M.F. Bachmann, Nanoparticles target distinct dendritic cell populations according to their size, Eur. J. Immunol. 38 (2008) 1404-1413.

[46] W.H. Fridman, F. Pagès, C. Sautès-Fridman, J. Galon, The immune contexture in human tumours: impact on clinical outcome, Nat. Rev. Cancer 12 (2012) 298-306.

Figure Legend

Figure 1 Preparation and characterization of mannose decorated chitosan nanoparticle encapsulation of tumor cell lysates. (A) Scheme of Man-ALG preparation. (B) FT-IR spectra of Man-ALG. (C) ^{1}H-NMR spectra of Man-ALG in D_2O. (D) The size distribution of Man-CTS-TCL NPs. (E) The TEM image of Man-CTS-TCL NPs. (F) Protein released from Man-CTS-TCL NPs in PBS at different pH values.

Figure 2 Mannose-decorated CTS-TCL NPs enhance bone marrow dendritic cells uptake of antigens *in vitro*. (A) DCs were incubated with FITC-labeled TCL, CTS-TCL NPs, and Man-CTS-TCL NPs for 4 h, then labeled with lysoTacker-Red to identify late endosomes and lysosomes, and labeled with DAPI for cell nucleus. The uptake of nanoparticles was detected by confocal microscopy. Scale bars, 25 μm. Data are representative of three independent experiments. (B-C) DCs were incubated with FITC-labeled TCL, CTS-TCL NPs, and Man-CTS-TCL NPs for 2, 4, 6, 12, 24 and 48 h, the histogram of mean fluorescence intensity (MFI) of BMDCs was detected by flow cytometry. Data are representative of three independent experiments. **P*<0.05, ***P*<0.01 and ****P*<0.001, Man-CTS-TCL NPs group compared with other groups.

Figure 3 Effect of mannose-decorated CTS-TCL NPs on mouse bone marrow dendritic cells maturation and antigen presentation *in vitro*. (A-B) Representative microscopic views of BMDCs maturation stimulated with TCL (A), Man-CTS-TCL NPs (B) for 48 h. Scale bar: 25 μm. (C-D) BMDCs were analyzed for expression of CD80, CD86, CD11c and CCR7 by flow cytometry after stimulated with TCL, Man-CTS NPs or Man-CTS-TCL NPs for 48 h. Data are representative of three independent experiments. (E-F) BMDCs were analyzed for expression of MHCI, MHCII, CD11c and CD40 by flow cytometry after stimulated with TCL, Man-CTS NPs or Man-CTS-TCL NPs for 48 h. Data are representative of three independent experiments, **P*<0.05, ***P*<0.01 and ****P*<0.001, Man-CTS-TCL NPs group compared with other groups.

Figure 4 *In vivo* tracking of Cyanine 7 labeled TCL, CTS-TCL NPs and

Man-CTS-TCL NPs in the injection site and draining lymph node. (A) Presence of TCL, CTS-TCL NPs and Man-CTS-TCL NPs in the injection site and the right inguinal draining lymph node, based on quantification of the fluorescent signal of near infrared coupled to the Cyanine 7. The lymph node is indicated by a red arrow. Repeated measurements in time plotted on the same scale of fluorescence. (B) The mean density of Cyanine 7 in the draining lymph node was calculated. All images are overlays of bright photographs with fluorescence intensity measurements indicated on the color scale. DLN, draining lymph node; ILN, inguinal lymph node. Data are representative of three independent experiments.

Figure 5 Effect of Man-CTS-TCL NPs induces immune responses in normal mice. (A) Draining lymph node was isolated at day 0 after s.c. injection of PBS, TCL, CTS NPs, Man-CTS NPs, CTS-TCL NPs and Man-CTS-TCL NPs in the right flank of C57BL/6 mice at day -14, -13 and -7, images of inguinal lymph node in different treatment groups. (B) Draining lymph node was made into single cell suspensions, and the expression of major DCs surface markers was analyzed by flow cytometry. (C-D) Antigen presentation in draining lymph node after immunized with PBS, TCL, CTS NPs, Man-CTS NPs, CTS-TCL NPs and Man-CTS-TCL NPs for 3 times *in vivo*. MHCI and MHCII antigen presentation was determined by measuring CFSE labeled $CD8^+$ T and $CD4^+$ T cell proliferation (defined as $CFSE^{low}$), respectively. (E) IFN-γ released from mice serum was tested by ELISA. (F) IL-4 released from mice serum was tested by ELISA. Data are representative of three independent experiments. Differences between Man-CTS-TCL NPs and other groups are analyzed using

one-way ANOVA analysis. *P<0.05, **P<0.01 and ***P<0.001, Man-CTS-TCL NPs group compared with other groups.

Figure 6 Man-CTS-TCL NPs vaccines induce protection effect in prophylactic tumor model. (A) Mean body weight during the total immunization course. (B) Mean tumor growth curves given by tumor volume. (C) The tumor weight was measured 21 days after last immunization. (D) Splenocytes were isolated 21 days after B16 tumor cells inoculation, co-cultured with B16 cells, and 3 days later used as effector cells for cytotoxic T lymphocytes (CTL) response assay. (E) Phenotype analysis of $CD3^+CD8^+$ T cells in mice lymph nodes 21 days after B16 tumor cells inoculation. (F) Phenotype analysis of $CD3^+CD8^+$ T cells in mice spleen 21 days after B16 tumor cells inoculation. Data are representative of three independent experiments. Bars shown are mean ± SD (n=6), and differences between PBS control group and other groups are determined using one-way ANOVA analysis and Student's t test. Relative to control groups: *P<0.05, **P<0.01 and ***P<0.001.

Figure 7 Man-CTS-TCL NPs vaccines confer therapeutic protection against melanoma. (A) Mean tumor growth curves given by tumor volume. (B) The tumor masses of each mouse on 22 days after B16 tumor cells inoculation. (C) The tumor weight was measured 22 days after tumor challenge. (D) Images of excised tumors from each mouse in each treatment group by the end of the assay. (E) IFN-γ released from serum of tumor bearing mice control, TCL, CTS NPs, Man-CTS NPs, CTS-TCL NPs and Man-CTS-TCL NPs groups was tested by ELISA. (F) Phenotype analysis of $CD3^+CD8^+$ T cells in mice spleen 22 days after B16 tumor cells inoculation. Data are

representative of three independent experiments. Bars shown are mean ± SD (n=6), and differences between PBS control group and other groups are determined using one-way ANOVA analysis and Student's t test. Relative to control group: *P<0.05, **P<0.01 and ***P<0.001.

Figure 1

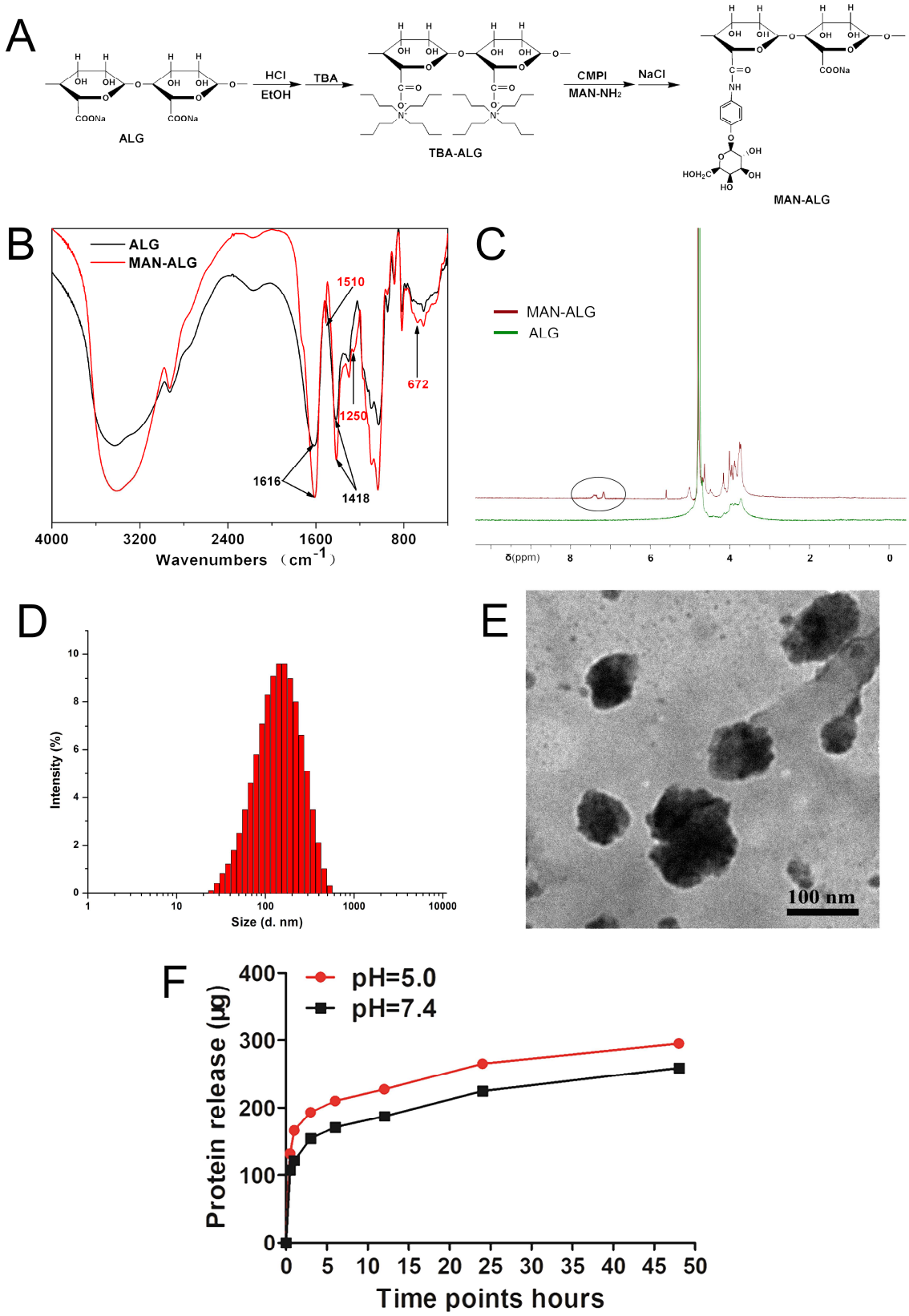
A
ALG
HCl
EtOH
TBA
TBA-ALG
CMPI
MAN-NH2
NaCl
MAN-ALG
B
ALG
MAN-ALG
1510
1250
672
1616
1418
Wavenumbers (cm-1)
C
MAN-ALG
ALG
δ(ppm)
D
Intensity (%)
Size (d. nm)
E
100 nm
F
pH=5.0
pH=7.4
Protein release (μg)
Time points hours

Figure 2

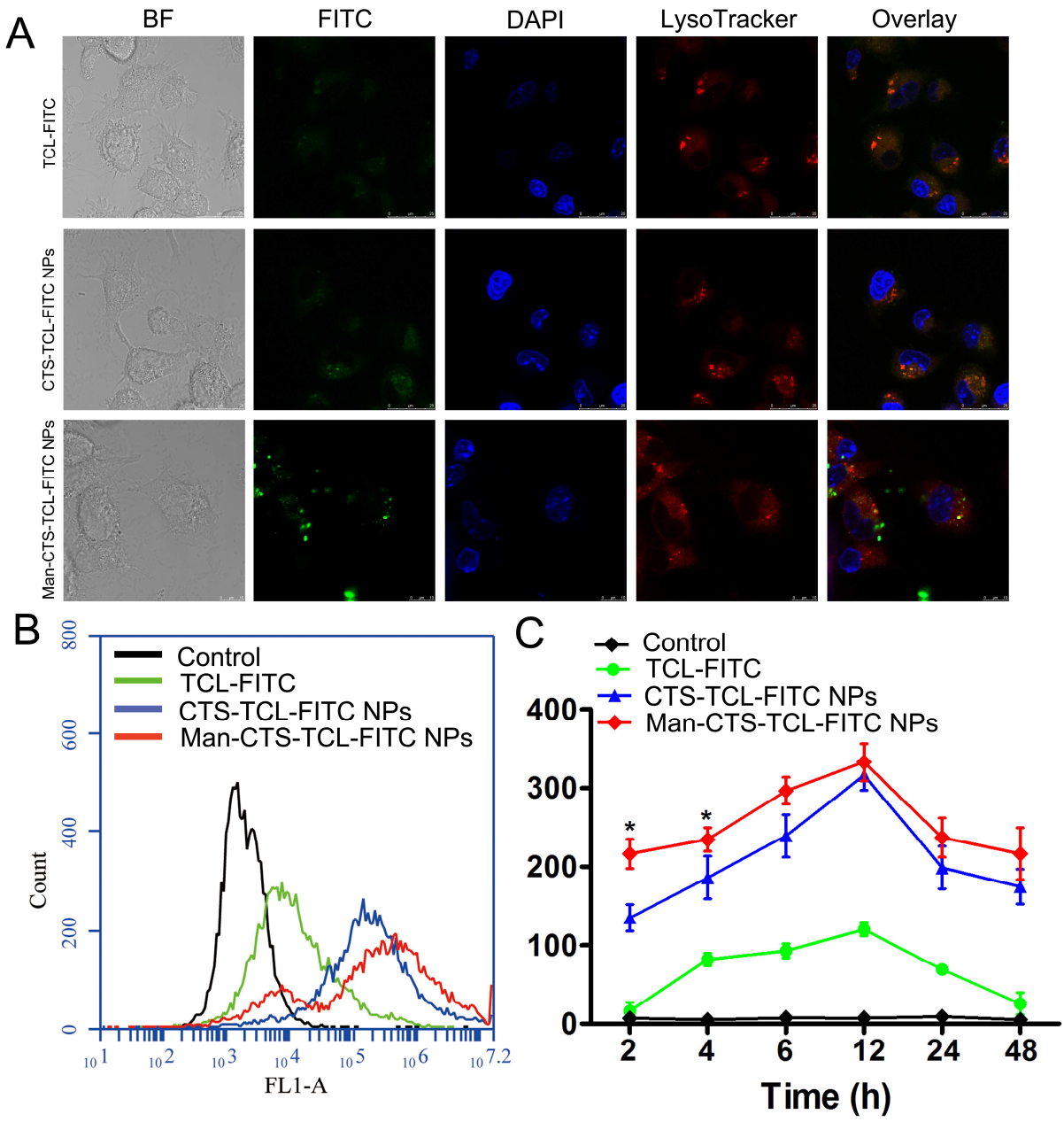
A
BF
FITC
DAPI
LysoTracker
Overlay
TCL-FITC
CTS-TCL-FITC NPs
Man-CTS-TCL-FITC NPs
B
Control
TCL-FITC
CTS-TCL-FITC NPs
Man-CTS-TCL-FITC NPs
Count
FL1-A
C
Control
TCL-FITC
CTS-TCL-FITC NPs
Man-CTS-TCL-FITC NPs
Time (h)

Figure 3

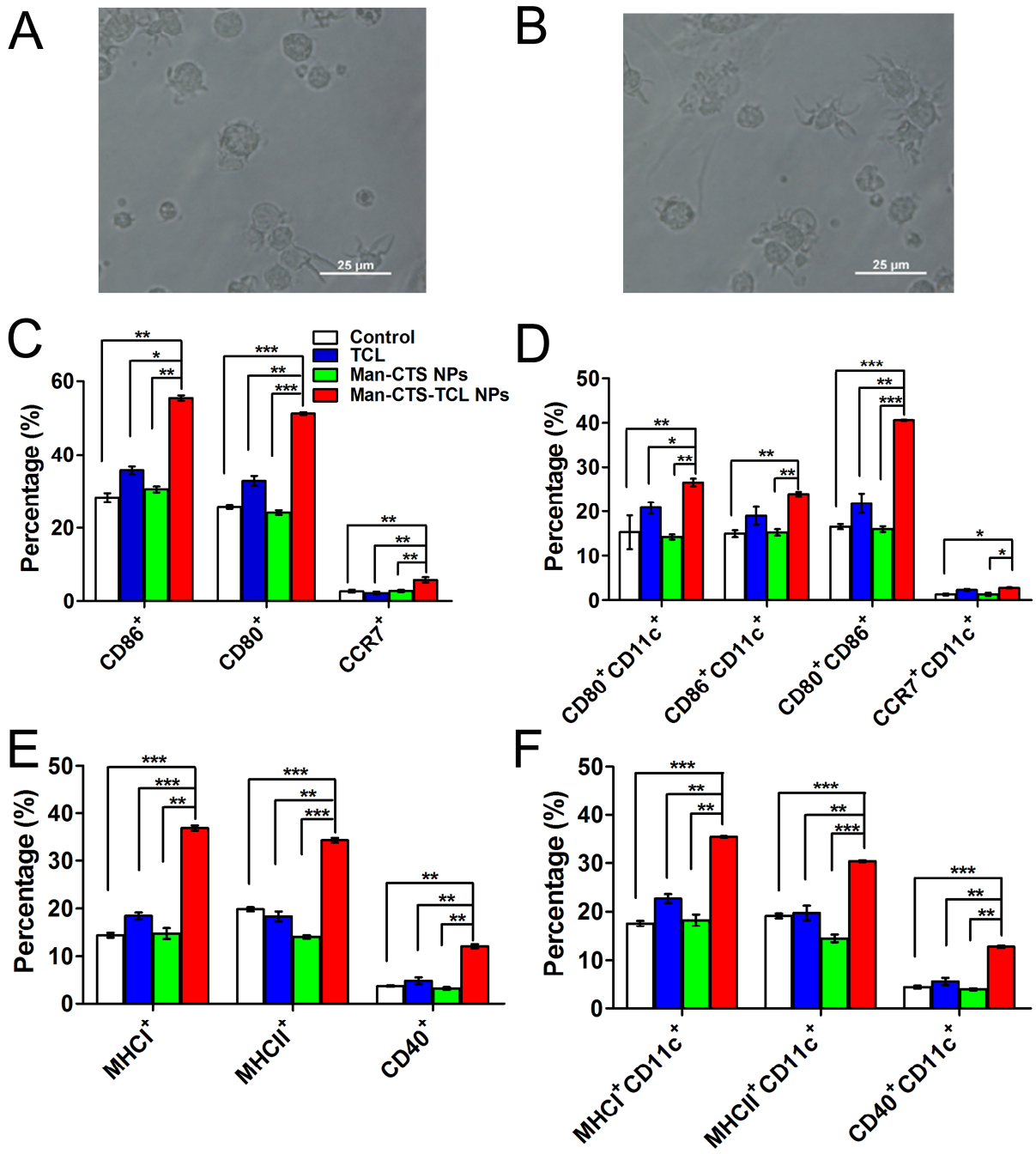
A
25 μm
B
25 μm
C
Control
TCL
Man-CTS NPs
Man-CTS-TCL NPs
Percentage (%)
CD86+
CD80+
CCR7+
D
Percentage (%)
CD80+CD11c+
CD86+CD11c+
CD80+CD86+
CCR7+CD11c+
E
Percentage (%)
MHCI+
MHCII+
CD40+
F
Percentage (%)
MHCI+CD11c+
MHCII+CD11c+
CD40+CD11c+

Figure 4

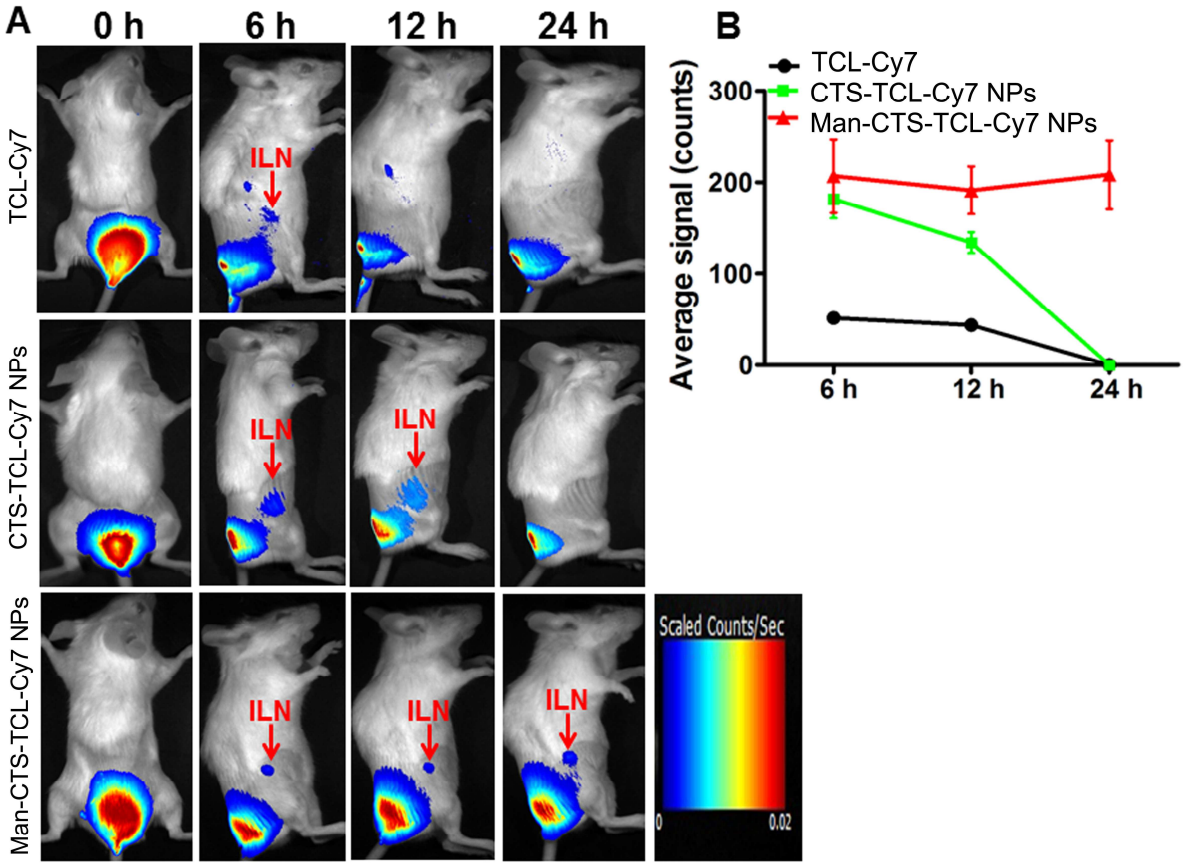
A
0 h
6 h
12 h
24 h
TCL-Cy7
CTS-TCL-Cy7 NPs
Man-CTS-TCL-Cy7 NPs
ILN
Scaled Counts/Sec
0
0.02
B
TCL-Cy7
CTS-TCL-Cy7 NPs
Man-CTS-TCL-Cy7 NPs
Average signal (counts)
300
200
100
0
6 h
12 h
24 h

Figure 5

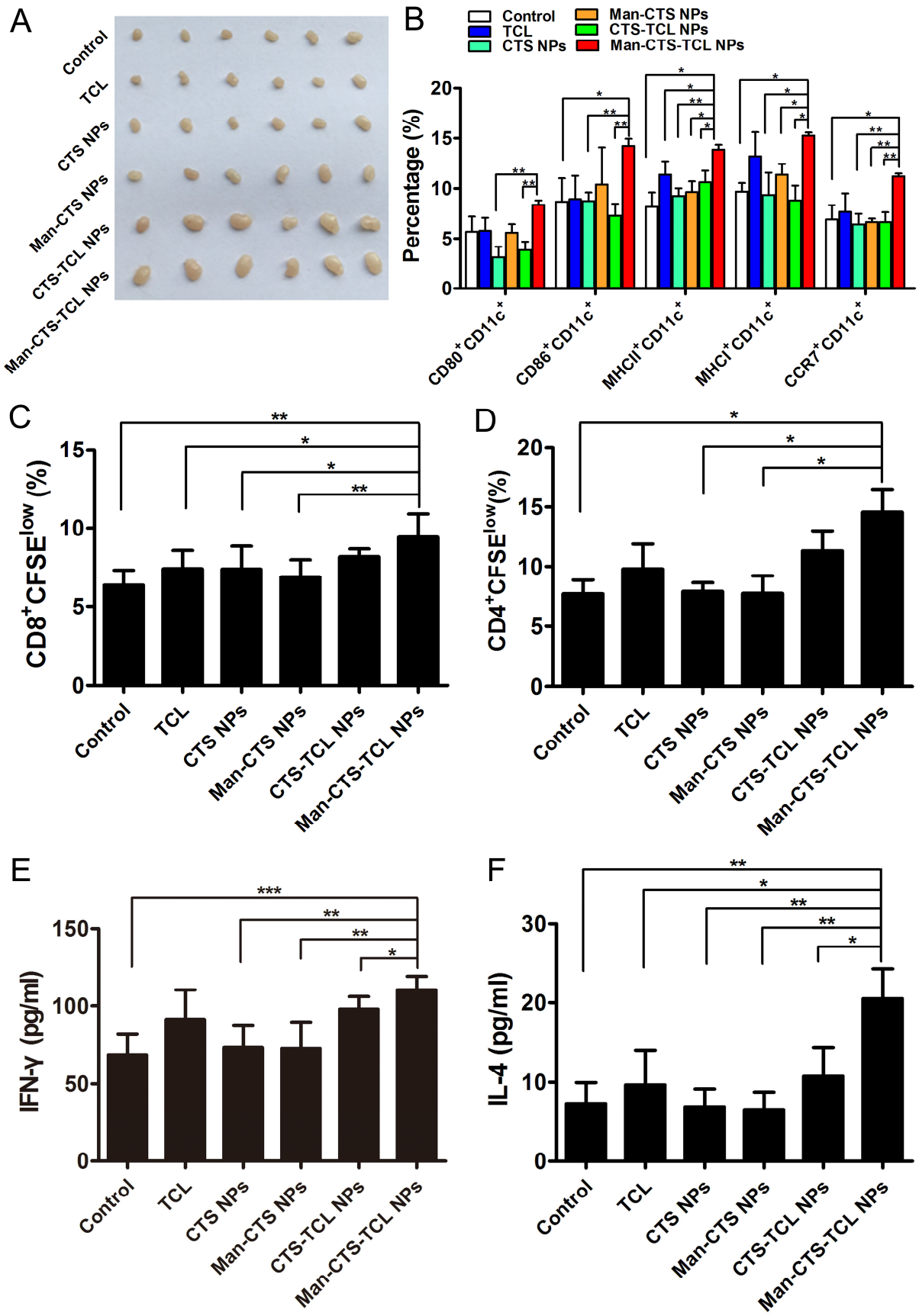
A
Control
TCL
CTS NPs
Man-CTS NPs
CTS-TCL NPs
Man-CTS-TCL NPs
B
Control
TCL
CTS NPs
Man-CTS NPs
CTS-TCL NPs
Man-CTS-TCL NPs
Percentage (%)
CD80+CD11c+
CD86+CD11c+
MHCII+CD11c+
MHCI+CD11c+
CCR7+CD11c+
C
CD8+CFSElow (%)
D
CD4+CFSElow(%)
E
IFN-γ (pg/ml)
F
IL-4 (pg/ml)

Figure 6

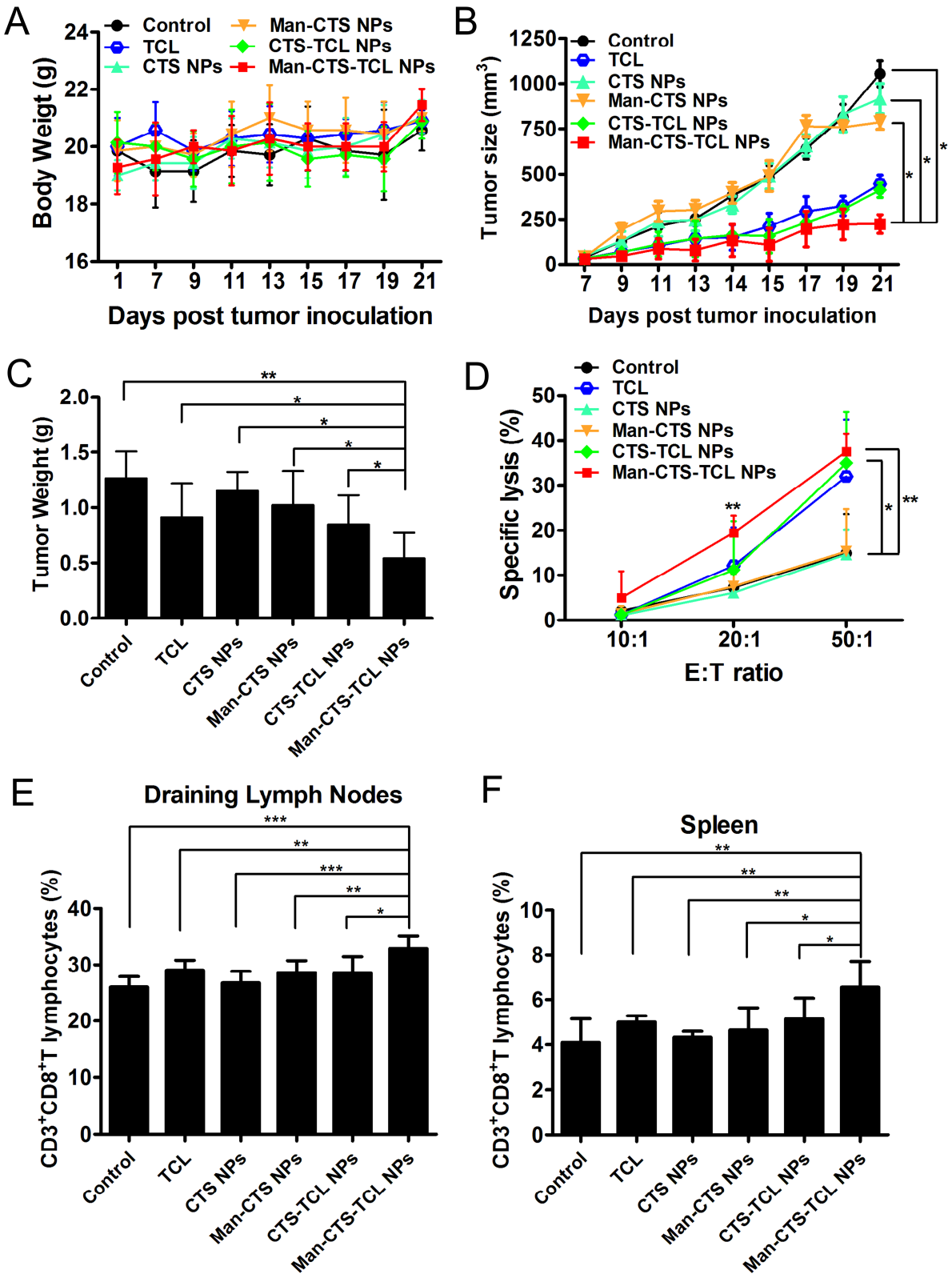
A
Control
TCL
CTS NPs
Man-CTS NPs
CTS-TCL NPs
Man-CTS-TCL NPs
Body Weigt (g)
Days post tumor inoculation
B
Tumor size (mm3)
Days post tumor inoculation
C
Tumor Weight (g)
D
Specific lysis (%)
E:T ratio
10:1
20:1
50:1
E
Draining Lymph Nodes
CD3+CD8+T lymphocytes (%)
F
Spleen

Figure 7

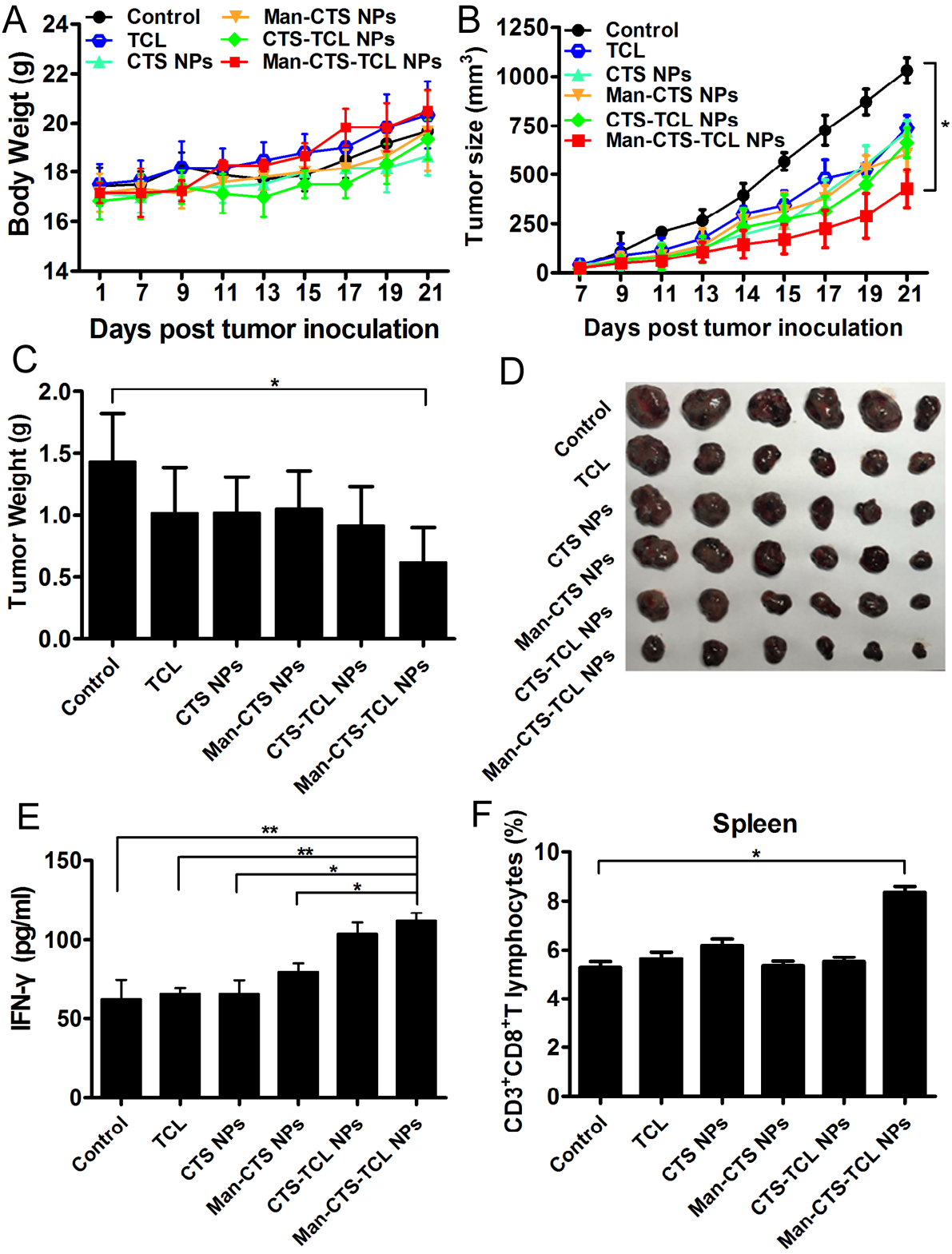
A
Control
TCL
CTS NPs
Man-CTS NPs
CTS-TCL NPs
Man-CTS-TCL NPs
Body Weigt (g)
Days post tumor inoculation
B
Tumor size (mm3)
Days post tumor inoculation
C
Tumor Weight (g)
D
E
IFN-γ (pg/ml)
F
Spleen
CD3+CD8+T lymphocytes (%)

Supporting Information for

Enhanced antitumor immunity by targeting dendritic cells with tumor cell lysate-loaded chitosan nanoparticles vaccine

Gao-Na Shia,1, Chuang-Nian Zhanga,1, Rong Xub, Jin-Feng Niuc, Hui-Juan Songa, Xiu-Yuan Zhanga, Wei-Wei Wanga, Yan-Ming Wangc, Chen Lia,**, Xiao-Qing Weid,***, De-Ling Konga,e,*

[a]Tianjin Key Laboratory of Biomaterial Research, Institute of Biomedical Engineering, Chinese Academy of Medical Science & Peking Union Medical College, Tianjin, 300192, China.

[b]Department of Clinical Infection Microbiology and Immunology, Institute of Infection and Global Health, University of Liverpool, L69 7BE, UK.

[c]State Key Laboratory of Medical Chemical Biology, College of Pharmacy and Tianjin Key Laboratory of Molecular Drug Research, Nankai University, 300353, China

[d]Cardiff Institute of Tissue Engineering & Repair, School of Dentistry, College of Biomedical and Life Sciences, Cardiff University, UK.

[e]Key Laboratory of Bioactive Materials, Ministry of Education, Nankai University, Tianjin 300071, China

[*] **Corresponding authors**

[**] **Corresponding authors**

[***] **Corresponding authors**

E-mail address: li0616826@126.com (C.Li), weiX1@cardiff.ac.uk (X-Q, Wei),

kongdeling@nankai.edu.cn (D-L, Kong) .

1 Gaona Shi and Chuangnian Zhang contributed equally to this work.

Experimental section

Preparation of FITC labeled tumor cell lysates (TCL-FITC)

Two mg of FITC in 1 mL of 20 mmol/L carbonate buffer (pH 9.5) added to a solution of TCL (1 mg/mL, 10 mL). The solution was incubated with continuous stirring at 4 ^{o}C for 18 h in the dark. The reaction mixture was dialyzed against distilled water (MWCO 1000) to obtain TCL-FITC.

Preparation and characterization of Man-CTS-TCL-FITC NPs

Three mL of TCL-FITC solution was added drop-by-drop into chitosan solution (1 mg/mL, 1% acetic acid) and mixed at 1:1 (w/w). The mixture was then agitated at 300 rpm for 30 min to obtain TCL-FITC loaded CTS nanoparticles (CTS-TCL-FITC NPs), which were collected by centrifugation and dissolved in PBS for experimental use. The Man-ALG solution (1 mg/mL) was added drop-by-drop into CTS-TCL-FITC NPs suspension to obtain mannose decorated CTS-TCL-FITC NPs (Man-CTS-TCL-FITC NPs) through electrostatic interaction. Man-CTS-TCL-FITC NPs were collected by centrifugation and suspended in PBS (pH 7.4) for further use.

Preparation of Cy7 labeled tumor cell lysates (TCL-Cy7)

Two mg of Cy7-NHS in 1 mL of 20 mmol/L carbonate buffer (pH 9.5) was added to a solution of TCL (1mg/mL, 10 mL). The solution was incubated with continuous stirring at 4 ^{o}C for 18 h in the dark. The reaction mixture was dialyzed against distilled water (MWCO 1000) to obtain TCL-Cy7.

Preparation and characterization of Man-CTS-TCL-Cy7 NPs

Three mL of TCL-Cy7 solution was added drop-by-drop into chitosan solution (1 mg/mL, 1% acetic acid) and mixed at 1:1 (w/w). The mixture was then agitated at 300 rpm for 30 min to obtain TCL-Cy7 loaded CTS nanoparticles (CTS-TCL-Cy7 NPs), which were collected by centrifugation and dissolved in PBS for experimental use. The Man-ALG solution (1 mg/mL) was added drop-by-drop into CTS-TCL-Cy7 NPs suspension to obtain mannose decorated CTS-TCL-Cy7 NPs (Man-CTS-TCL-Cy7 NPs) through electrostatic interaction. Man-CTS-TCL-Cy7 NPs were collected by centrifugation and suspended in PBS (pH 7.4) for further use.

Results section

Table S1. Characterization of nanoparticles (n=3).

Sample	Size (nm)	DPI	Zeta potentials (mV)
CTS-TCL NPs	127.46±6.73	0.114±0.031	-14.07±1.22
Man-CTS-TCL NPs	120.15±9.93	0.121±0.049	-12.07±1.36
CTS-TCL-FITC NPs	134.72±2.65	0.103±0.051	-15.41±1.25
Man-CTS-TCL-FITC NPs	136.18±7.63	0.131±0.047	-14.58±1.19
CTS-TCL-Cy7 NPs	139.16±10.03	0.119±0.039	-15.46±1.52
Man-CTS-TCL-Cy7 NPs	135.48±8.97	0.124±0.041	-14.92±1.43

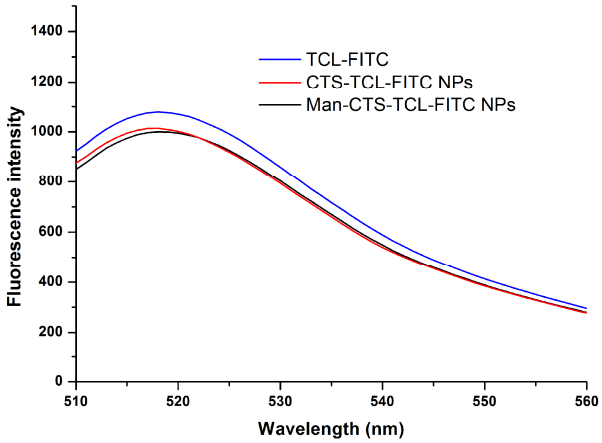

Figure S1The fluorescence spectra of TCL-FITC, CTS-TCL-FITC NPs and Man-CTS-TCL-FITC NPs in PBS, and the excitation wavelength is 495 nm.

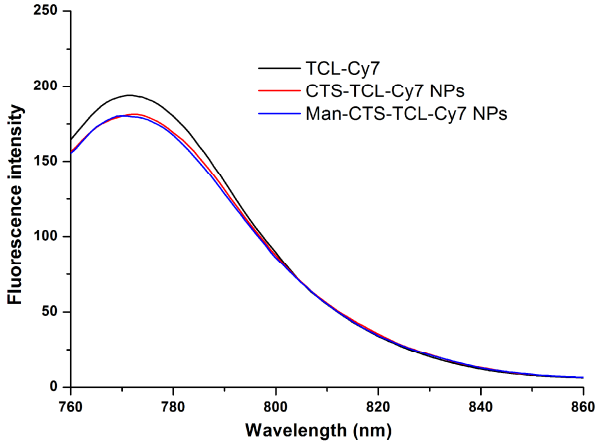

Figure S2 The fluorescence spectra of TCL-Cy7, CTS-TCL-C NPs and Man-CTS-TCL-Cy7 NPs in PBS, and the excitation wavelength is 743 nm.

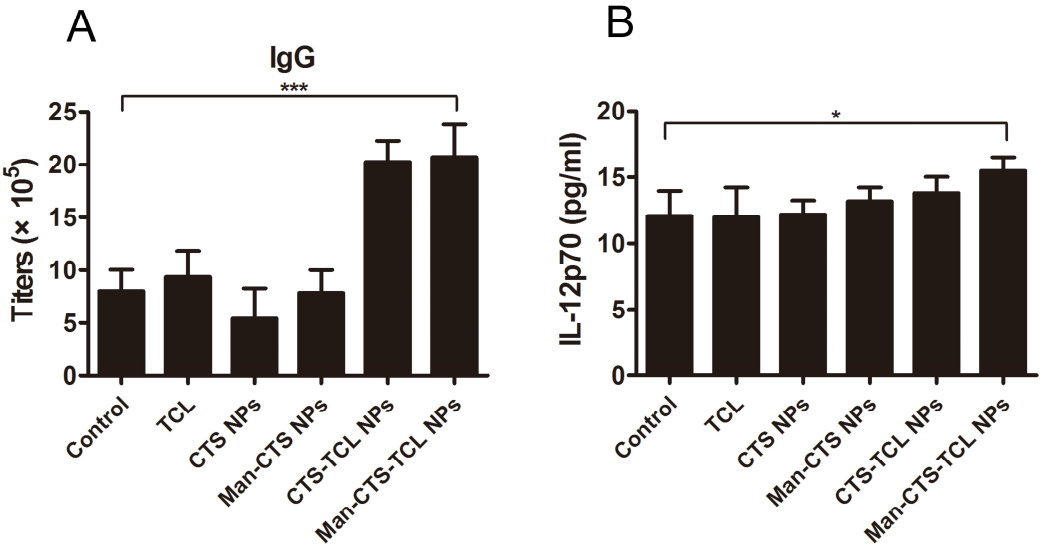

Figure S3 Immunization with Man-CTS-TCL NPs produces both cellular and humoral immune responses in mice. (A) Female C57BL/6 mice (n=6) 6-8 weeks old were subcutaneously immunized with PBS, TCL, CTS NPs, Man-CTS NPs, CTS-TCL NPs and Man-CTS-TCL NPs at days -14, -13, and -7. At day 0, serums of mice were collection and assayed for tumor specific IgG antibody (humoral immune response) by ELISA. (B) Serums of mice were used for measuring IL-12p70 (cellular immune response) by ELISA. Data are representative of three independent

experiments. Bars shown are mean ± SD (n=6), and differences between PBS control group and other groups are determined using one-way ANOVA analysis and Student's t test. Relative to control group: *P<0.05, **P<0.01 and ***P<0.001.

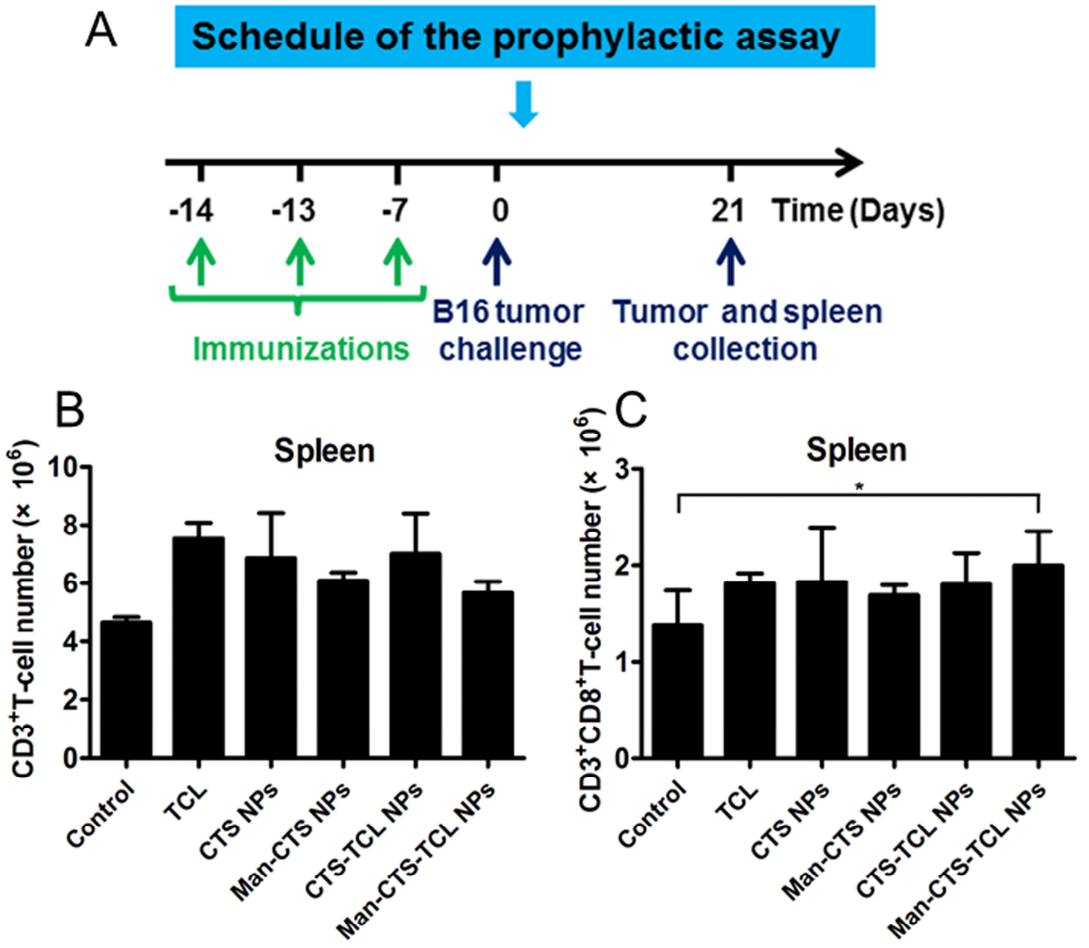

Figure S4 Immunization of mice with Man-CTS-TCL NPs enhances the absolute number of $CD3^+CD8^+$ T cells in mice spleen. (A) Schedule used for the prophylactic assay. (B) Number of CD3+ T cells (C) and CD3+CD8+ T cells isolated from spleen 21 days after B16 tumor cells inoculation. Data are representative of three independent experiments. Bars shown are mean ± SD (n=6), and differences between PBS control group and other groups are determined using one-way ANOVA analysis and Student's t test. Relative to control group: *P<0.05, **P<0.01 and ***P<0.001.

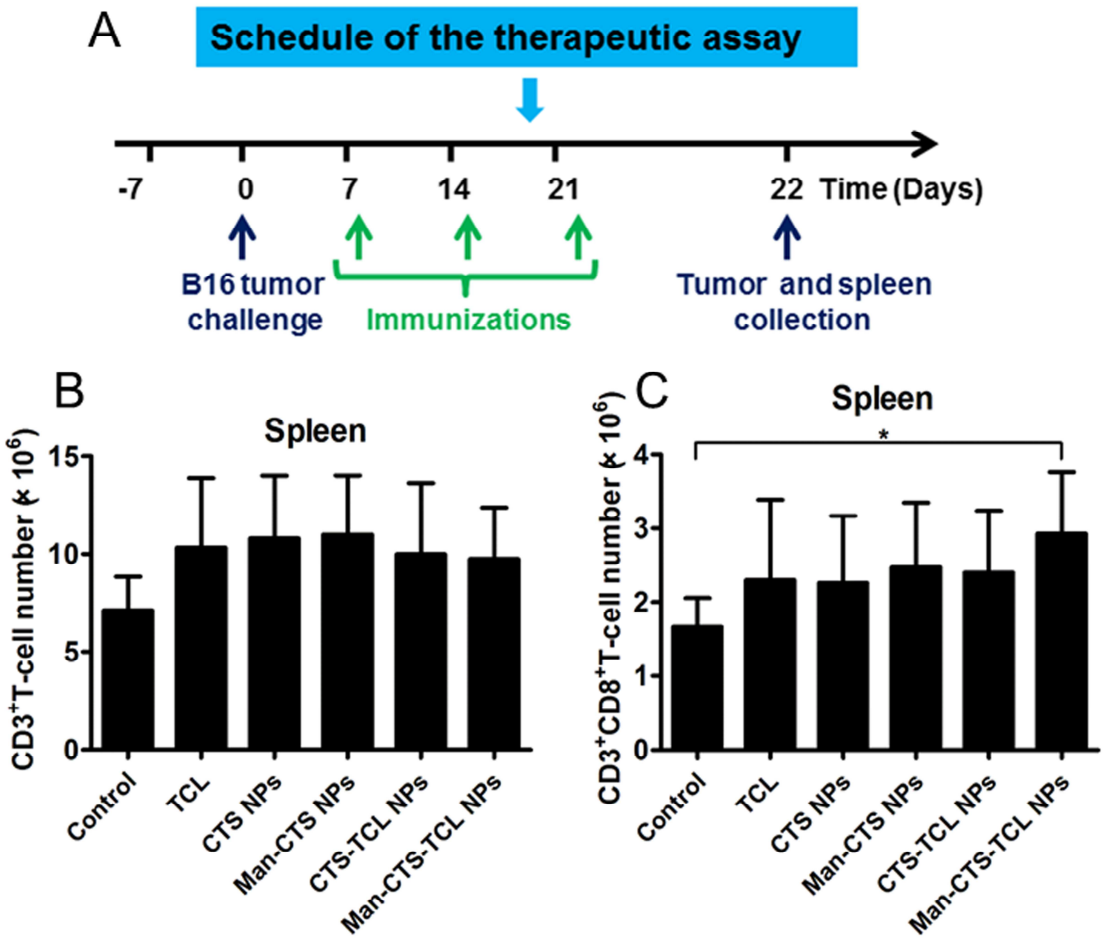

Figure S5 In the therapeutic tumor model, Man-CTS-TCL NPs possesses higher level of the absolute number of $CD3^+CD8^+$ T cells in mice spleen. (A) Schedule used for the therapeutic assay. (B) Number of $CD3^+$ T cells (C) and $CD3^+CD8^+$ T cells isolated from spleen 22 days after B16 tumor cells inoculation. Data are representative of three independent experiments. Bars shown are mean ± SD (n=6), and differences between PBS control group and other groups are determined using one-way ANOVA analysis and Student's t test. Relative to control group: $*P<0.05$, $**P<0.01$ and $***P<0.001$.